

# Analysis of Atmospheric Mesoscale Models for Entry, Descent and Landing

D. M. Kass,<sup>1</sup> J. T. Schofield,<sup>1</sup> T. I. Michaels,<sup>2,4</sup> S. C. R. Rafkin,<sup>2,4</sup> M. I. Richardson,<sup>3</sup> A. D. Toigo,<sup>3,5</sup>

## Abstract.

Each Mars Exploration Rover (MER) is sensitive to the martian winds encountered near the surface during the Entry, Descent and Landing (EDL) process. These winds are strongly influenced by local (mesoscale) conditions. In the absence of suitable wind observations, wind fields predicted by martian mesoscale atmospheric models have been analyzed to guide landing site selection. In order to encompass the available models and render them useful to the EDL engineering team, a series of statistical techniques were applied to the model results. These analyses cover the high priority landing sites during the expected landing times (1200 to 1500 local time). The number of sites studied is limited by the computational and analysis cost of the mesoscale models.

The statistical measures concentrate on the effective mean wind (the wind as seen by the landing system) and on the vertical structure of the horizontal winds. Both aspects are potentially hazardous to the MER landing system. In addition, a number of individual wind profiles from the mesoscale model were processed into a form that can be used directly by the EDL Monte-Carlo simulations.

The statistical analysis indicates that the Meridiani Planum and Elysium landing sites are probably safe. The Gusev Crater and Isidis Basin sites may be safe, but further analysis by the EDL engineers will be necessary to quantify the actual risk. Finally, the winds at the Melas Chasma landing site (and presumably other Valles Marineris landing sites) are dangerous.

While the statistical parameters selected for these studies were primarily of engineering and safety interest, the techniques are potentially useful for more general scientific analyses. One interesting result of the current analysis is that the depth of the convective boundary layer (and thus the resulting energy density) appears to be primarily driven by the existence of a well organized mesoscale (or regional) circulation—primarily driven by large scale topographic features at Mars.

## 1. Introduction

The Mars Exploration Rover (MER) Entry, Descent and Landing (EDL) process is sensitive to wind speeds and wind shears expected for at least some locations on Mars. This has required explicitly studying the winds that may be encountered during the landing process to ensure that the EDL system is robust for the specific sites of interest. The EDL system is primarily sensitive to winds and wind shear from when the parachute is deployed ( $\sim 7$  km) to the surface, although the winds as high as 30 km will influence the landing location and extreme winds in these regions could hamper the EDL system [Crisp *et al.*, this issue].

The EDL system can have problems with horizontal winds as low as 10 m/s in the lowest  $\sim 5$  km, with failures very likely above

25 m/s. The sensitivity to wind shear is more difficult to quantify, because of the complex, frequency dependent, response of the spacecraft while descending on the parachute. There are several systems that have been implemented to potentially mitigate the effects of wind. Without these, the EDL system is sensitive to even more modest winds and wind shear [Crisp *et al.*, this issue].

The MER EDL system is similar to Mars Pathfinder (MPF), but several changes conspire to make the MER landing significantly more difficult. The MER lander mass is much greater than for MPF. MER will be landing in the early afternoon, when convective activity is at its peak whereas MPF landed in the early morning hours when the atmosphere is expected to be less turbulent and often calmer. Furthermore, MPF landed at  $\sim -4$  km (relative to the MOLA aeroid [Smith *et al.*, 2001]—all altitudes are referenced to the MOLA aeroid) whereas MER is required to be able to land at elevations as high as  $-1.3$  km.

The sensitivity of the MER EDL system to winds necessitated a good understanding of the winds expected at various potential landing sites to ensure they would be safe. Unfortunately, there are few actual observations of the martian winds, primarily because winds in the equatorial regions are difficult to observe from orbit and while both Viking Landers and MPF had surface meteorology stations, they only measure the winds in the lowest few meters. This led to the use of martian mesoscale model results [Rafkin *et al.*, 2001; Toigo and Richardson, 2002] to study the winds at potential landing sites.

<sup>1</sup>Jet Propulsion Laboratory, California Institute of Technology, Pasadena, California, USA

<sup>2</sup>San Jose State University, San Jose, California, USA

<sup>3</sup>California Institute of Technology, Pasadena, California, USA

<sup>4</sup>Now at: Southwest Research Institute, Boulder, Colorado, USA

<sup>5</sup>Now at: Cornell University, Ithaca, New York, USA

Mesoscale models are the best available tool to provide estimates for the winds in the regions of the atmosphere of interest in the absence of observations. They are currently the only type of model that can properly resolve the winds in the convective boundary layer over realistic topography at the resolutions of interest. The fact that they are non-hydrostatic is particularly important for calculating correct wind velocities in convective systems [Pielke and Pearce, 1994].

It was necessary to run the mesoscale models with very high resolution grids ( $< 2$  km) in order to analyze the wind shear at the important wavelengths. Very large data sets result when the model domains are sufficiently large to cover the regions of interest. Furthermore, the inherent complexity of the models and the high resolutions necessary severely limit the length of the model runs (most cases were run for four sols, one sol for spinup and three sols of valid results).

The large size of the model data sets required significant analysis to reduce the information to a form usable by the MER EDL engineering team. This resulted in a series of statistical analyses of the mesoscale model results of interest to extract the aspects important for EDL. While the statistical techniques and parameter choices described here are specifically designed for engineering purposes, they do reveal several scientifically interesting results. And the techniques can be modified to study properties more directly of scientific interest.

Two independent mesoscale models were used in the MER EDL analyses. The first model is the MRAMS model, described by Rafkin *et al.* [2001] and the second is the Mars MM5 model, described by Toigo and Richardson [2002]. The details of the modeling performed for EDL is in Toigo and Richardson [this issue] and Rafkin and Michaels [this issue]. While both models have a long heritage in terrestrial mesoscale modeling, both are only recent adaptations for Mars. Two models were used to allow validation by intercomparison (when the studies started, both models were brand new and neither had seen significant use or validation). The decision was further driven by the critical nature of the winds to the MER EDL systems, since errors could result in the loss of the spacecraft and all their potential science.

The basic approach was to analyze the wind speed and wind shear independently. This resulted in separate statistical parameters for each property, and implicitly assumed that they are statistically independent (but the actual parameters are still valid even if they are correlated; the interpretation just becomes more complex). The speed was characterized by the effective (or mean) wind speed. The shear (vertical shear in the horizontal winds) was characterized by a pair of parameters, one measuring long vertical wavelength shear and the other for short wavelength shear. The particular parameters selected have the equally important advantage that their effects on the EDL system are expected to be independent. The results indicate that while there is some correlation among the wind properties, treating them independently is not unreasonable. The use of randomly selected wind profiles from the mesoscale models in some of the engineering analyses helps account for any interdependence.

## 2. Effective Wind Speed

The effective wind is a measure of the mean (or sustained) wind over the altitude of interest to the EDL process. The effective wind entrains the parachute (and lander with it) during the descent, resulting in a net horizontal velocity when the lander actually touches the surface. This velocity must then be removed by the airbags,

bringing the lander to rest. There is a limit to the total velocity the airbags can effectively absorb [Crisp *et al.*, this issue].

### 2.1. Method

For any given wind profile, the following integration is applied to determine the effective wind for each component:

$$E_x = \frac{\int_a^b x(z) \exp\left(-\frac{z-a}{c}\right) dz}{\int_a^b \exp\left(-\frac{z-a}{c}\right) dz} \quad (1)$$

Where  $x(z)$  is the wind velocity component of interest ( $u$ : westerly,  $v$ : northerly or  $w$ : upwards) as a function of altitude  $z$ ,  $a$  is the starting altitude and  $b$  is the ending altitude.  $c$  is the parachute response wavelength ( $c \sim 1500$  m for the MER EDL system). For the MER landers, the integration was performed from 100 m to 5100 m. This is effectively a weighted mean with an exponential decrease in the weighting with altitude. It represents the response of a system descending on a parachute to a varying wind field, where the effects of higher altitude winds are damped out by those nearer to the surface. It is also numerically equivalent to a low pass filter for a simple, linear parachute. This is easily implemented numerically on a discrete wind field (simple first order box integration with each grid point as the midpoint—more sophisticated integration methods could be applied but the uncertainty in the model results makes it unnecessary).

The integration is sufficiently general and any parameter could be used. For MER EDL, the main application was to determine the effective horizontal wind speed ( $E_s$ ). This was obtained by calculating the effective velocity of each horizontal wind component ( $E_u$  and  $E_v$ ) and then calculating the resulting wind speed. Note that this is not the same as calculating the wind speed at every altitude and the applying the integral (which gives a significantly higher value and fails to take wind direction into account).

The results of integrating the vertical wind ( $E_w$ ) are not overly interesting for EDL purposes. In this case, grid points were averaged in two groups: one with upwards winds and one with downwards winds. Otherwise mass balance will often result in a near zero mean. In both models, but especially the Mars MM5 model, the vertical averages varied noticeably from (output) timestep to timestep. This was especially apparent at the Meridiani Planum site and is apparently due to convective systems “drifting” through the analysis region, significantly varying the structures being averaged. Unfortunately, with only a few timesteps (except for the MRAMS Meridiani Planum study), there is still significant noise in the averages. The mean wind values seen in the models are not a concern to the MER EDL system. But the distributions are strongly non-Gaussian and have significant extremes. Excluding Meridiani Planum, even the extreme values are not significant to the landing system. At Meridiani, the individual profile analyses (see Section 6) have indicated that the vertical winds are not a problem. Overall, the vertical winds are somewhat more difficult to interpret and thus will not be discussed further.

### 2.2. Analysis Regions

A family of profiles representing the MER landing conditions (local time and geographic location) was selected from each mesoscale model for each landing site. These profiles were then used for all of the statistical analyses (as well as for selecting individual profiles).

The mesoscale model output is generally stored hourly. To insure that the expected variability in conditions with local time was covered, model timesteps between 12:00 and 15:00 LTST (local true solar time) were selected. This usually resulted in 3 timesteps per sol (and with 3 sols of usable results, a total of 9 timesteps). Note that the actual number of timesteps selected varies from site to site (depending on the number of sols of results available and the phasing in local time of the stored timesteps, which varies depending on the model starting time and longitude of interest—effectively there is one phasing for each landing site).

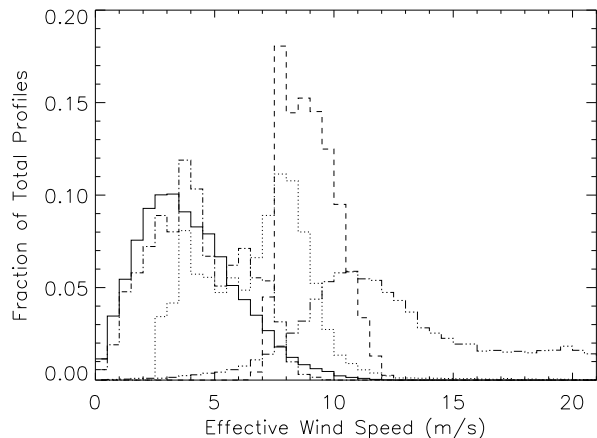


**Figure 1.** Model Mean Wind Speed Histogram. This figure shows a histogram of the effective wind speed (m/s) distribution for some of the landing sites. These are shown in 0.5 m/s bins as a fraction of the total number of profiles analyzed. The solid line is for the Meridiani Planum, the dotted line for the Gusev Crater site, the dashed line for the Isidis Basin site, the dash-dotted line for the Elysium Planitia site, and the dash-triple-dot line for the Melas Chasma site (no longer under consideration). The Melas Chasma winds slowly decrease above 20 m/s, with the highest speeds around 30 m/s.

In addition to selecting the relevant times, the analysis was limited to the expected landing ellipse. For most ellipses, this was done by defining a box enclosing the ellipse (or at least the parts of the ellipse within the model grid). For the Meridiani Planum site, an explicit list of points was created to avoid selecting points within a nearby crater. This was not necessary for the other sites (based on the modeled topography and studies of the resulting wind fields, all of the nearby locations included are similar to the ellipse itself).

The families of profiles defined for each landing ellipse by this process were also used for all the other analyses. The resulting region is fairly generic and covers both the opening and closing ellipses as well as (for the relevant sites) both the MER-A and MER-B ellipses. Note that while the two landers arrive at slightly different seasons, all of the mesoscale models were run for the MER-A arrival seasons. The MER-B arrival season is not expected to be significantly different and it was not computationally possible to cover the two separate seasons in the time available.

The trajectory during the entry process is not vertical, and actually starts almost horizontal [Crisp *et al.*, this issue]. But by the time it reaches the altitudes of interest for the wind analysis, it is nearly vertical. An analysis shows that, given the grid spacing of the model results, the atmosphere along the spacecraft trajectory is well represented by simply using a vertical profile and only tracking the spacecraft's altitude.

### 2.3. Wind Speed Results

Figure 1 shows the histogram of  $E_s$  (see eq. 1) for each of the potential landing sites analyzed. While not perfect, the effective speeds are approximate beta distributions, the expected result for Gaussian  $u$  and  $v$  components. This allows the mean and variance (or standard deviation) to be meaningfully calculated (these are shown in Table 1).

While not overly useful for EDL purposes, it is also possible to produce a hodograph using the effective velocities (Figure 2). This clearly shows the influence of the regional topography on each

landing site. Some sites (Isidis) have very well defined wind directions and velocities while others (Meridiani Planum) are much more variable.

While the constants used in the calculations presented in this paper are specific for the MER EDL system, any landing system using a parachute (one of the more effective ways of landing) is likely to have similar constants. Thus these results are probably relevant to any lander attempting to land at the  $L_s$  and local time of the MER landers. And more importantly, the analysis techniques are directly applicable to any attempts to land on Mars.

In addition to the engineering application of these results, studies like those shown in Figure 2 can be useful for understanding the results of mesoscale models. For example, it shows that while the horizontal winds at Meridiani Planum (a) have a generally random direction, the region does appear to have northeasterly wind bias (or preferences), which is probably indicative that the convective systems are drifting in that direction. While an exponential weighting function is probably not the ideal one to use to study this, it is simple to insert a different weighting function in Equation 1.

### 3. Vertical Structure

The vertical structure of the martian wind fields (shear, turbulence and other vertical variability) represents a significant hazard to the MER EDL system. While extremes (for example a dust devil) might

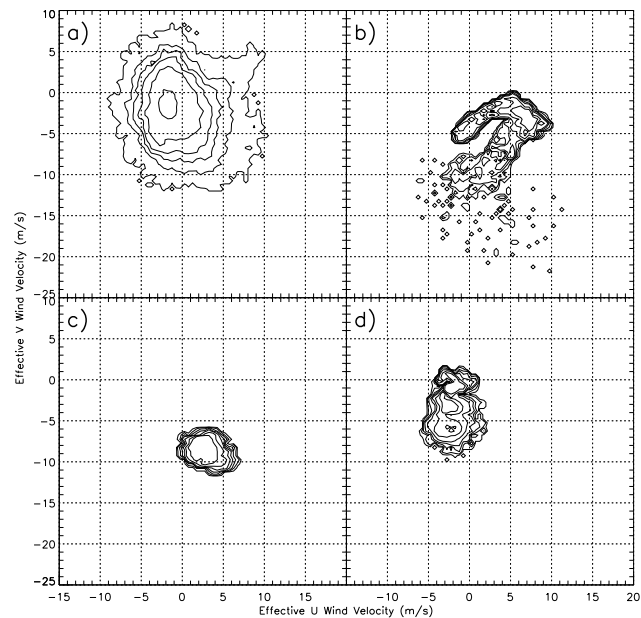


**Figure 2.** Wind Speed Hodographs. Each figure shows the ensemble of effective wind velocities at one of the landing site. Each location in the figure represents the tip of the effective wind vector for a mesoscale profile, with North being at the top of the figure and East being to the right. The effective  $u$  and  $v$  component winds of each profile are calculated, placing the profile in the effective wind space of the figure. Then the ensemble of profiles for each site was contoured (due to the large numbers involved), using a 0.5 m/s bin (in each direction). The outermost contour encompasses all the regions with any profiles, the next contour encompasses regions with 0.02% of the profiles per bin. Succeeding profiles encompass 0.05%, 0.1%, 0.2%, 0.5% and 1% of the profiles per bin. (a) is the Meridiani Planum site, (b) is the Gusev Crater site, (c) is the Isidis Basin site and (d) the Elysium Planitia site.

cause mechanical failures, these types of events are very unlikely (due to the rapid entry and small “footprint”) and the spacecraft is designed to physically withstand most normal variability. Unfortunately, the vertical structure also causes the lander to sway like a pendulum. This causes the retro-rockets (RADS) to not fire vertically, causing them to impart a horizontal velocity on the lander. There are a number of different modes that the spacecraft can oscillate in while landing. Two of the more dangerous ones (for the purposes of landing) are an overall pendulum motion of the entire system and a high frequency oscillation of the backshell containing the RADS known as the “evil mode” within the EDL community [Crisp *et al.*, this issue].

Due to the vertical grid spacing of the mesoscale models, the two regimes are analyzed separately, using different techniques. The “pendulum mode” is sensitive primarily to oscillations with vertical wavelengths of  $\sim 1.5$  km and greater. The “evil mode” is sensitive to wavelengths of  $\sim 350$  m to  $\sim 1000$  m [Crisp *et al.*, this issue].

In the shear analyses, the winds (and atmosphere) can be thought of as “frozen” so that temporal variability need not be considered. This is due to the high speed during entry ( $> 70$  m/s while on the parachute). As the spacecraft passes through the atmosphere, it only samples a point location, so it maps any existing time variability into a vertical variability.

### 3.1. Mars Pathfinder Model

The first difficulty in analyzing the vertical shear in the mesoscale models is in describing it in a format that is convenient for Monte-Carlo EDL modeling. For historical reasons, the EDL engineering team started studying shear issues using the Mars Pathfinder Wind Model (MPF model) [Smith *et al.*, 1995].

The MPF model is a simple power spectral density model. It is based on terrestrial data taken at Cape Kennedy and the theoretical form of clear air turbulence. There is an “expected” martian scaling factor applied to make the single axis standard deviation 5 m/s. It has the following form:

$$G_u(f) = 2.4 \times 10^{-4} f^{-2.4} + 0.01 f^{-5/3} \frac{(\text{m/s})^2}{(\text{cycles/m})} \quad (2)$$

The frequencies ( $f$ ) are those from a Fourier series starting at 163 km, using a 5 km to 20 m bandpass. The amplitudes and phases are then generated randomly and summed at each altitude grid point. This is done for each wind axis ( $u$  and  $v$ ) [Smith *et al.*, 1995].

For modeling convenience (and historical development), shear (and other vertical variability) were described in terms of an MPF model scaling factor (called the MPF scaling factor). This is just the scaling factor that multiplies the MPF model to produce shear equivalent to the analyzed mesoscale results. It only applies, of course, to the range of vertical spatial frequencies being analyzed.

By comparison to the mesoscale model results, the long wavelength slope was found to be a good fit for Mars (at least as represented by the mesoscale models). This also matches the theoretical expectations for martian turbulence [Kieffer *et al.*, 1992]. There was no way to test the model slope at high frequencies not sampled by the observations or the mesoscale models, but it is expected to be reasonable to the same extent that clear air turbulence theory is reasonable [Pielke and Pearce, 1994].

### 3.2. Long Wavelength Shear

In the context of the EDL analysis of the mesoscale models, the long wavelength shear refers to the variability with altitude of the horizontal wind fields that is explicitly expressed by the model results. The mesoscale models have a vertically varying grid spacing over the regions of interest [Rafkin and Michaels, this issue; Toigo and Richardson, this issue]. Thus the actual spatial wavelengths are not obviously defined.

#### 3.2.1. Fourier Analysis.

In order to examine the explicit shear in the mesoscale model, a Fourier transform was performed on each wind profile. This is a spatial transform in the vertical direction, thus the result is the power at various vertical wavelengths. The  $u$  and the  $v$  components of the wind were transformed independently.

The transform was done numerically, after interpolating the wind profile to a 10 m vertical grid. The region between 100 m and 5210 m was used (allowing for 512 points for an efficient transform). For each wavelength between 5120 m and 731 m, the ratio of the magnitude of the resulting spectrum from each profile to the magnitude of the MPF model expected spectrum was calculated. The resulting multiplicative factors were averaged over the wavelength to define the long wavelength scaling factor for each wind component of the profile.

While individual profiles often show distinctly dominant wavelengths, the mean spectrum is very smooth (Figure 3). This indicates a lack of dominant large scale organizations of the vertical structure—at least in the lowest 5 km. The MPF model also exhibits this behavior (by construction), making it a reasonable representation. Thus, while the calculated deviations at individual wavelengths is quite large, all profiles will oscillate around the mean. No profile has an extreme behavior at every wavelength.

#### 3.2.2. Shear Results.

To insure a conservative parameter, the larger of the two component scaling factors was defined as the one for the entire profile. In most of the sites, the two directions showed similar factors (when averaged over the ensemble of the site). This indicates that, according to the models, the long wavelength shear is generally isotropic at the sites of interest. The anisotropy seen at some sites is probably due to the preferential direction of the mean flow. Since only some of the sites with a strong mean flow show an anisotropy, a closer study of the shear parameter could reveal regions with subtly different responses to topographic and solar forcing.

The short wavelength cutoff was chosen partly based on the actual grid spacing and partly on looking at the roll-off in the individual

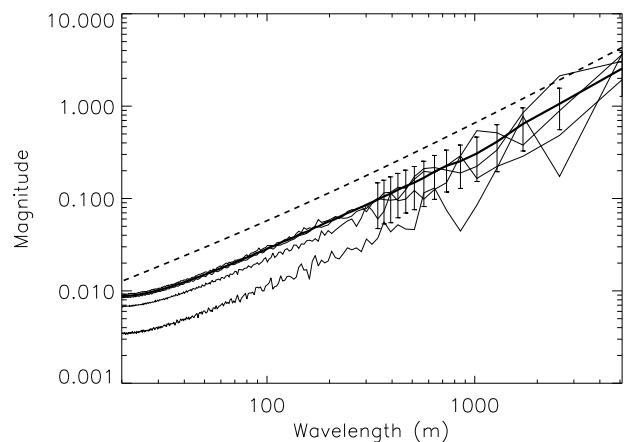


**Figure 3.** Spectral Analysis of several wind profiles from Gusev Crater. This figure shows the results of the Fourier analysis (showing the magnitude of the spectrum versus its wavelength—in m) of a few individual profiles from the Gusev Crater landing site (thin lines). The thick solid line is the average of the spectra of all the individual profiles for the landing site, the error bars show the (one standard deviation) range of individual spectra at each wavelength. The dashed line is the spectrum of the MPF wind model for comparison.

and composite spectra (Figure 3). While this is shorter than the “pendulum mode,” it is an attempt to constrain the “evil mode” as much as possible with the available model results.

Overall, the long wavelength shear seen in the models is modest in highly convective regimes (Table 1). On the other hand, sites dominated by regional circulation patterns (e.g., Gusev Crater) can show significant vertical structure.

### 3.3. Short Wavelength Turbulence

Unfortunately, the wavelengths of variability that drive the “evil mode” are not well represented by the mesoscale model results. Due to the EDL system design they are, unfortunately, likely to be the most important in determining the horizontal velocity induced by the RADS.

In the MRAMS model [Rafkin *et al.*, 2001], the TKE (turbulent kinetic energy) is explicitly calculated and saved as one of the output parameters. It represents the integrated energy in the turbulence (or variability) of the winds at wavelengths shorter than explicitly represented by the model grid. This was used as a proxy for the variability at the wavelengths of interest.

#### 3.3.1. TKE Scaling.

As it is an integrated quantity, the TKE does not provide any information on the wavelength dependence of the turbulence. Nor does it provide any information on the direction of the turbulence (if it is not isotropic).

It was necessary to convert the TKE values to a scaled quantity useful to the engineers. This was achieved by calculating the TKE of the MPF model [Holton, 1992] over the range of wavelengths the TKE represents in the mesoscale models (up to wavelengths of  $\sim 300\text{m}$ ). The TKE in the MPF model is per axis so it was multiplied by a factor of three to correspond to the full 3 dimensional nature of the mesoscale models. This results in an expected TKE value of  $\sim 1.5\text{ m}^2/\text{s}^2$ . This value was then used to convert all of the statistical TKE properties into an MPF scaling factor.

This scaling process implicitly assumes that the MPF short wavelength slope of  $-5/3$  from boundary layer theory applies to Mars. Furthermore, the TKE calculated from the MPF model is truncated at wavelengths of 20 m, whereas that in the mesoscale models extends to shorter wavelengths. Some simple studies extending the MPF model to finer wavelengths indicate that there is little total energy at the shorter wavelengths and ignoring them is not unreasonable.

#### 3.3.2. TKE Analysis.

One of the important features of the mesoscale models is that the turbulence (as shown by the TKE fields and other indicators) primarily extends over the convective boundary layer and is almost zero elsewhere. There are exceptions, as expected, for strong shear zones (e.g., Gusev Crater) at other altitudes. These are ignored for the following discussion (and are “reintroduced” later).

Several statistical parameters related to TKE were calculated over the analysis sets. The simplest was the average peak TKE. The maximum TKE value in each profile was found and these were averaged. This parameter was calculated because the “evil mode” has minimal damping so the location of the altitude of the excitation is mostly irrelevant. But when used as a scaling factor for the MPF model, this still results in a significant overestimate of the excitation of the EDL system.

The second parameter studied for each landing site was the average of mean TKE of each profile over the turbulent (or convective) boundary layer. This was calculated by finding the top of the boundary layer—defined as the point above which the TKE value dropped below 10% of its peak value. The examination of a number of individual profiles showed this to be an effective measure. Then the TKE field between the surface and the boundary layer top was averaged for each profile (and converted to an MPF scaled equivalent).

This was found to work well in representing the short wavelength variability. As a side benefit, although not of interest for EDL purposes, this method results in a boundary layer height for each profile. The mean boundary layer height at each landing site helps explain some of the more interesting trends observed.

#### 3.3.3. TKE Results.

Unfortunately, the TKE primarily represents wavelengths shorter than the “evil mode.” This made it difficult to directly apply the TKE scaling factors to the EDL system behavior. They are useful for site to site comparisons and help provide a bound on the possible turbulence.

The EDL simulation team found that an average of the long wavelength shear factors and the mean TKE factors did give a reasonable representation of the overall system performance. But this issue became moot with the introduction of actual mesoscale model profiles.

## 4. Model and Site Intercomparisons and Results

Table 1 contains a summary of the statistical analyses of the some of the landing sites under consideration for MER. These are the seven locations where at least one of the mesoscale models was run for the MER landing season. The Elysium Planitia site model run only contains part of the current (EP78B2) landing site and most of that is potentially contaminated by “edge effects.” Thus the nearby EP78B site ( $\sim 30\text{ km}$  south) was analyzed (the model was run before the new site had been selected). Studying the limited available data indicates that the two sites are virtually identical as far as the winds are concerned. The Schiaparelli Crater site is an ellipse positioned at the equator and 15 East. This is not a possible site due to the elevation (and probably also the geophysical properties). The mesoscale model was run at this location for a regional study (see the next section). At the Meridiani Planum site, the MRAMS model output was stored every 10 minutes.

### 4.1. Model Uncertainty

There are some basic differences between the two models that are reflected in the tabulated results. In particular, the two use different vertical grids, different gridding schemes and different closure schemes [Rafkin and Michaels, this issue; Toigo and Richardson, this issue]. Among other effects, this appears to change the distribution of the energy between shear and turbulence. This is partly a resolution issue (in terms of the vertical wavelengths that can be resolved). Unfortunately, it is not easy to verify the differing energy distributions since the Mars MM5 model (in the version used for these simulations—note that the Isidis run used a slightly different version of the Mars MM5 code) does not have a convenient parameter corresponding to the TKE field. In general, the Mars MM5 model is expected to have lower shear parameters. Another difference between the two models is in the atmospheric dust loading. The MRAMS model used a fixed value ( $\tau \sim 0.3$ ), while the Mars MM5 model uses interactive dust transport (partly controlled by the GCM). While difficult to compare, due to the variability in the Mars MM5 model, it appears that the latter has a slightly higher average opacity.

The two mesoscale models show quite good agreement at the Meridiani Planum site. This is probably due to the smooth topography, allowing thermal convection to dominate the circulation. There is also reasonable agreement at the Isidis Basin site where the wind regime is dominated by the sharp southern basin rim. The agreement is less good at Gusev Crater and Melas Chasma, but both were very challenging topographically. In particular, the Mars MM5 run

Statistical Analysis Summary							
	Wind Speed			Shear	Variability		
	Horizontal	Up	Down		Turbulence (TKE)		Thickness
	m/s	m/s	m/s		MPF	Scale Factor	
Meridiani Planum (TM10A2/TM10B2)							
MRAMS	4 ±2	2.5	1.1	0.4	0.7	1.2	4.8
Mars MM5	4 ±2	1.4	1.7	0.2			
Gusev Crater (EP55A2)							
MRAMS	7 ±2	0.4	0.2	0.9	1.8	2.1	1.7
Mars MM5	3 ±1	0.3	0.3	0.5			
Isidis Basin (IP84A2/IP96B2)							
MRAMS	9 ±1	0.6	0.4	0.7	2.0	2.4	2.4
Mars MM5	11 ±2	0.2	0.2	1.4			
Elysium Planitia (EP78B2/EP78B)							
MRAMS	4 ±2	0.6	0.3	0.3	1.5	1.8	2.1
Melas Chasma (VM53A2/VM53B2)							
MRAMS	14 ±5	0.7	0.8	0.8	1.6	2.8	
Mars MM5	1*±1	0.1	0.1	0.5			
West Elysium Planitia (EP80B2)							
MRAMS	6 ±2	0.4	0.3	0.4	1.6	1.8	
Schiaparelli Crater							
MRAMS	2 ±1	0.6	0.2	0.2	1.5	1.7	

\* Speeds are significantly higher 2 hours later (6 ±3 m/s, see text)

**Table 1.** Summary of all the statistical analyses. The “Shear” is the long wavelength variability while the “Turbulence” is the short wavelength (TKE based) variability (see text). Schiaparelli Crater is not an actual ellipse but a location in the crater (see text), for the other sites, the specific ellipses covered are indicated in parentheses [Golombek *et al.*, this issue]. The uncertainty given for the horizontal wind speeds are the formal  $1\sigma$  values. The formal uncertainty in the MPF scaling factors is similar to that of the MPF model (and thus subsumed in the definition). In addition, all values have the factor of two uncertainty inherent in the mesoscale modeling (see text). The Mars MM5 model was not run at all the locations and also does not contain the output for TKE analysis.

at Melas Chasma was so computationally expensive that the model had to be somewhat simplified. While the overall diurnal cycle is similar to that seen in MRAMS, it is offset by about 2 hours in local time [Toigo and Richardson, this issue; Rafkin and Michaels, this issue], possibly due to the computational simplifications. When the offset is accounted for (by performing the statistical analysis between 14:00 and 17:00 LTST), the two models show moderate agreement at the Melas Chasma site (note that the vertical winds and shear also increase). It is also possible that in addition to the time offset, the simplification resulted in a reduction in the wind speeds. In the case of Gusev crater, the wind is stronger towards the end of the period, suggesting a similar behavior.

There are several possible explanations for the differences. It is interesting that the two locations with weaker model agreement are locations where the GCM does not resolve the important topographic features. This may have more of an impact on the Mars MM5 model due to the smaller horizontal domains used in the modeling [Toigo and Richardson, this issue]. It is also possible that the higher opacity in the Mars MM5 model is partly causing the differences. The dust amount (and distribution) could be affecting the phasing of the winds and/or their strength.

Based on the model intercomparison, the lack of observations for validation in the regions of interest, the state of the mesoscale models, and the quality of the input data sets, we feel that the model results (at least in the statistical sense studied here) are valid to within a factor of two. In most of the cases, the two models agree better than this. In the cases where the models only agree to within a factor of two (or are slightly worse), there are a number of issues that would appear to partly explain the differences. It is important to remember that both of the mesoscale models used have long histories in the terrestrial atmospheric community. Thus the fundamental physics is unlikely to be wrong, and while the martian experience is limited, there is a significant understanding of how mesoscale models perform in general.

Many of the causes of error are likely to be systematic (at least beyond what is seen and unexplained between the two models). These are they types of errors that are difficult to gauge without

observations to use for comparisons. While such systematic errors might have different magnitudes at different sites, they would still change all of the model results in the same direction. Thus differences smaller than a factor of two may be relevant when evaluating the sites relative to each other (for example in ranking them from the safest to the most dangerous site).

## 4.2. Site Safety

Based on the statistical analyses and site intercomparisons, it is possible to put the potential landing sites into three broad groups. While one could theoretically use a finer scheme, the uncertainty in the models limits the ability to distinguish between sites. The model results clearly distinguish between Meridiani Planum and Melas Chasma (their important parameters are over a factor of two different), but it is much more difficult to distinguish between some pairs of sites. For example, while the turbulence parameters are higher for Elysium Planitia than Meridiani Planum, this is bordering on the resolution of the models. And, when coupled with the similar horizontal winds, it is probably not possible to distinguish between them in terms of landing safety on the basis of the winds.

When classifying sites, it is necessary to consider not only the mean values but also the variance. Both can be important in terms of evaluating spacecraft safety. This is because the spacecraft performance (or probability of landing successfully) is mostly insensitive to the winds below a threshold ( $\sim 10$  m/s for horizontal winds), then decays slowly, but it finally reaches a point after which it degrades rapidly ( $\sim 25$  m/s). It is more difficult to determine when the shear and turbulence are dangerous (since they do not map directly into the system performance). In general, if both are elevated, the site is probably dangerous, otherwise it is somewhat based on engineering judgment (and best tested using the actual profiles as discussed in section 6). While the mean can be marginally acceptable, a broad distribution can make a significant fraction of the winds too dangerous, thus making the entire site overly dangerous. Furthermore, due to the engineering nature of the study, it is necessary to be conservative. Thus we generally look at the more dangerous of the

two models for each site (this is the MRAMS model everywhere but at Isidis). As noted earlier, the vertical winds have not been found to discriminate between the sites and will be ignored for this discussion.

The first group contains sites that are likely to be “wind safe.” This includes both the Meridiani Planum and the Elysium Planitia sites. Both sites have low horizontal winds that are safe even if the models are a factor of two low on estimating the wind speed. Nor are the tails of the wind distributions (see Figure 1) dangerous. The Elysium site has moderate to high turbulence, but it still has low shear and is thus likely to be safe. While not currently under consideration for a landing site, the Schiaparelli Crater location also falls in this category (although as mentioned previously, the actual location studied has other problems that make it unsuitable for landing). The West Elysium Planitia site is quite similar to the main Elysium site and we consider it to be a “wind safe” site. Although perhaps it is not quite as safe as the other three sites. The two Elysium sites are relatively close and in similar regional settings, thus the model errors should be similar for both sites. Therefore, we feel that the difference in horizontal wind speed is probably significant. When combined with the elevated turbulence (shared by both Elysium sites), the site is starting to have a number of non-optimal wind conditions. This leads us to conclude that the West Elysium Planitia site is probably not quite as safe as the other “wind safe” sites.

The second group are sites that are questionable. These sites contain one or more aspects of the wind regime that may push the limits of the landing system. A site can also be questionable if several parameters are moderate. Isidis Basin and Gusev Crater fall in this category. In the case of Gusev Crater, all of the wind parameters are roughly a factor of two worse than at Meridiani. While the mean wind is perhaps not quite a factor of two worse, the distribution (see Figure 1) is bimodal and has a surprisingly long tail (extending to over 20 m/s). The Isidis Basin site shows a strong mean horizontal wind (distinguishably stronger than at Meridiani, for example), but unlike Gusev Crater the distribution is very narrow without any outliers. In both cases, the mean wind speeds are borderline if one assumes the models are a factor of two low (and in the case of Isidis basin, the good agreement between the two mesoscale models implies that they are likely to be more accurate than a factor of two). The shear and turbulence at both sites is quite high, but are estimated to be borderline for the MER EDL system. These sites require additional EDL engineering analysis to better understand their impact on landing safety. Note that the ultimate safety may also depend on other site properties [Golombek *et al.*, this issue].

Finally, there are unsafe sites such as Melas Chasma. The Melas Chasma site has shear and turbulence parameters similar to Gusev Crater and Isidis Basin, which are reaching the limits of landing system. The slightly lower mean turbulence combined with the higher peak turbulence implies that there are some very strong layers of turbulence within the boundary layer, although this may not be statistically significant. While the mean wind at Melas Chasma is only slightly higher than at Isidis (14 m/s versus 11 m/s for the conservative model for each site), the variance at Melas Chasma is significantly larger. At a statistical  $2\text{-}\sigma$  level, the Melas Chasma winds are into dangerous territory while the Isidis winds are still acceptable (24 m/s versus 15 m/s). In the actual model results (see Figure 1), the difference is even more striking. Isidis lacks the “tail” seen at Melas Chasma (which extends to  $\sim 30$  m/s). When the implications of the “tail” are combined with the elevated shear and turbulence parameters, Melas Chasma must be considered a dangerous site. It should be noted that other site properties (especially the local topography [Golombek *et al.*, this issue]) are likely to combine very unfavorably with the strong winds and shear in Melas Chasma.

#### 4.3. Boundary Layer Thickness

The convective boundary layer on Mars can grow to a significant height (as measured by the TKE thickness parameter), but it does

not always do so. It appears that this is strongly a function of the mesoscale (or regional) wind regime. Based on the limited sites examined in these studies, there seem to be at least two, and possibly three, types of regimes, characterized by different heights.

The first type of location are ones where the regional winds are light/non-existent. In this case, in the mid-afternoon, the boundary layer will grow to its “full” height ( $\sim 5$  km). The Meridiani Planum site is a good example of this behavior. Analysis of the modeling of the site [Rafkin and Michaels, this issue; Toigo and Richardson, this issue] indicate that it is dominated by convective activity. This is also apparent in the random nature of the wind directions (see Figure 2).

On the other hand, a strong regional wind (such as those generated at Isidis Basin site by the basin rim and North/South dichotomy [Kieffer *et al.*, 1992]) will suppress the convective boundary layer and keep it fairly shallow. It appears that the advection of the convective cells deforms them, presumably limiting their height. It is also possible that depth of the katabatic flow itself limits the convection (by “shearing” the top off as the cells are advected by the near surface flow as the atmosphere above is slower)[Rafkin and Michaels, this issue; Toigo and Richardson, this issue]. The Melas site may show an extreme example of this phenomena with its multiple layers with different flow directions (in particular the probably remnant of the nighttime katabatic flow in center of the canyon [Rafkin and Michaels, this issue]).

Note that while the Elysium Planitia site has wind speeds similar to Meridiani Planum, they are driven by the North/South dichotomy and are not controlled by an active convective system (see Figure 2). Thus it is actually a site with a regional wind and a boundary layer thickness is similar to what is seen at the Isidis site. This implies that even a modest regional flow is capable of influencing the boundary layer thickness. The more northerly latitude, and thus less insolation, (the sub-solar latitude is  $\sim 13^\circ$  South at the season of the simulations) of the Elysium site may also contribute to the thinner boundary layer, but it does not appear that this is sufficient to explain the reduction in boundary layer thickness seen.

The possible third regime is represented by the Gusev Crater case. In this case, there is a very strong, complex and varying flow within the crater. In addition to the strong topographically driven horizontal flow, there is a significant downwelling over the landing site [Rafkin and Michaels, this issue; Toigo and Richardson, this issue] which would further suppress the height of the convective system. The net result is a very shallow boundary layer. Without a significantly wider sampling of locations (and especially locations with the same insolation), it is unclear if the boundary layer thickness at Gusev is controlled by the subsidence or by the horizontal flow.

One interesting aspect of these suppressed boundary layers is the enhanced turbulence within them revealed by the mean (or peak) TKE. Since all the sites are equatorial, they receive similar (but not identical) insolation. The variable energy input does make simple quantitative comparisons impossible. The differences in boundary turbulence is presumably due to a general conservation of energy. Basically the surface heating drives a more or less fixed amount of atmospheric convective energy (for a given site). In a thick boundary layer, this energy is spread out so the energy density is low. In one of the suppressed layers, the energy cannot spread out as much, resulting in higher TKE values. This is obviously not the only process in effect. This can be seen by comparing the Isidis Basin and Elysium Planitia sites, both northerly and having similar boundary

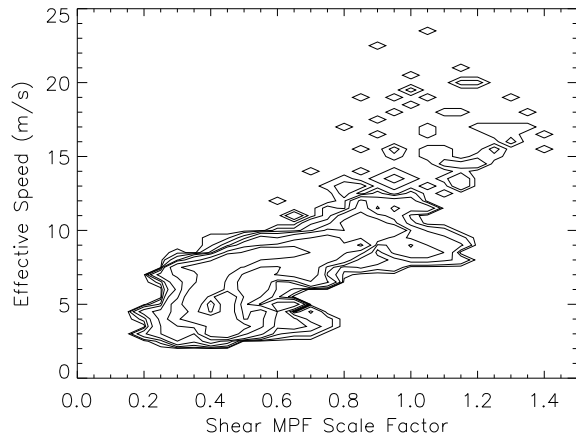


**Figure 4.** Gusev Crater Wind Statistics. The figure shows a contour of the values of the long wavelength shear and effective wind speed for the Gusev Crater site. The outermost contour encompasses all the regions with any profiles, the next contour encompasses regions with 0.02% of the profiles per bin. Succeeding profiles encompass 0.05% profiles per bin, 0.1%, 0.2%, 0.5% and 1% of the profiles per bin.

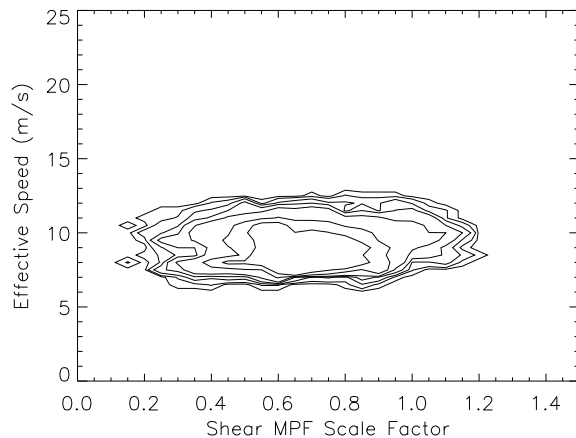


**Figure 5.** Isidis Basin Wind Statistics. The figure shows a contour of the values of the long wavelength shear and effective wind speed for the Isidis Basin site. The contours are identical to the ones used in Figure 4

layer thicknesses and yet significantly different turbulence fields). Other processes that might be involved include the flow “concentrating” energy (by keeping the atmosphere in contact with the surface for longer periods) or the effect of the interactions of higher wind speeds with the surface roughness.

#### 4.4. Parameter Independence

Figures 4 and 5 show the relationship between mean wind speed and wind shear (long wavelength) for the Gusev Crater and Isidis basin landing sites. These sites show the range of independence of the wind speed and wind shear across the various sites. The correlation coefficient between the two fields is 0.68 for Gusev Crater and lower for the other sites (0.55 at Meridiani, 0.26 for Elysium and 0.04 for Isidis). In the case of Gusev, much of the correlation is

driven by the high speed and high shear outliers (the selected contour spacing tends to exaggerate this population). If one removes the extreme 15% (wind speeds above 9 m/s and shear values above 0.8), the correlation coefficient drops to 0.45 (the Meridiani correlation also drops when the outliers are removed). The correlation is probably due to stronger winds being more capable of supporting larger shear features.

Overall, the initial assumption of independence of the wind speed and wind shear is borderline for Gusev, but robust for the other sites. Partly to insure that this weak correlation was captured, actual pro-

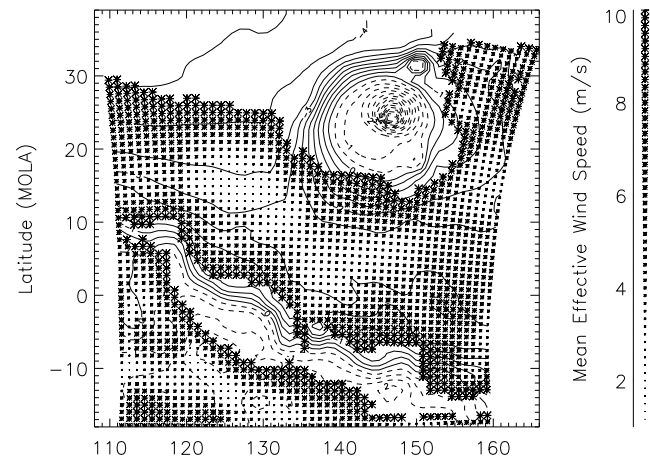


**Figure 6.** Elysium Regional Analysis of the Effective Wind Speed. This figure shows the mean effective wind speed (m/s) at each grid point of the MRAMS grid 2 according to the scale bar. The model topography ( $\sim 1$  degree MOLA topography) is contoured (1/2 km interval; contours above the 0 km elevation are dashed). A number of high wind regions are shown as blank to preserve the details in the low wind regions of interest for EDL studies.

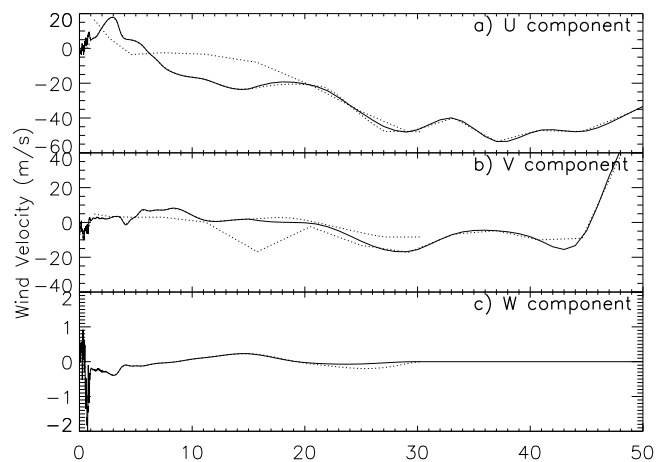


**Figure 7.** Profile Generation Process. This figure shows the three wind components ((a)  $u$ , (b)  $v$ , and (c)  $w$ ) as an engineering wind profile is generated. This is a profile from the Gusev Crater landing site. In all three directions, the altitude along the profile is shown from the surface to 50 km. Note that the wind velocity changes scale between the two horizontal and the vertical component. The solid line is the final generated profile. The two dotted lines are the MRAMS profile (surface to 30 km) and the Ames MGCM profile (1.5 km and up) used to generate this profile. Note that the vertical winds in the MGCM are small and are assumed to be zero (and are not shown).

files from the mesoscale models were used in some of the engineering analyses (see section 6). Given the actual correlations observed, we feel that the independent analyses are useful and relevant for this study. Note that the individual parameters are completely valid if correlated, it is just the analysis and understanding of the implications for the landing system that are more difficult.

Figures similar to Figure 5 were found to be very useful for EDL engineering analyses. The expected approximate probability of success for various EDL system configurations (e.g., parachute design) could be mapped into the same parameter space due to the selected parameters having independent effects on the EDL system. By superimposing the statistical wind results, the effects of the spacecraft design and winds could be rapidly evaluated [Crisp *et al.*, this issue].

## 5. Regional Scale Studies

The same analysis techniques discussed in the previous sections as applied to the high resolution mesoscale model results within the landing sites can be applied to lower resolution grids (and models). This was particularly useful in searching for another low wind site [Golombek *et al.*, this issue].

In this case, the MRAMS grid 2 ( $\sim 60$  km horizontal grid spacing) was analyzed (Figure 6). One issue in such cases is the local time since it will vary over the model domain. Due to the quantization (and hourly sampling) of the model, a simple selection for the desired three hour window results in artifacts (e.g. the abrupt transition at  $135^\circ$  longitude). These can obviously be eliminated by smoothing or a finer model sampling, but were just ignored in the site search.

Figure 6 shows the mean effective wind for the model run, but the other profile parameters can also be studied. The spectral terms (and TKE), not shown, are misleading unless the horizontal grid scale is taken into account. Also, in some of the fields, the higher resolution nested grids also create artifacts. This is due to the lower resolution overlapping grid actually being an average of the higher resolution region [Rafkin *et al.*, 2001].

A slightly different approach was to use the extreme value for a location instead of the average. This was particularly useful in looking for low wind regions by locating areas with occasionally excessive winds that may have a reasonable mean wind, but have a long tail to the distribution of parameters.

Regional scale statistical studies may also be useful in mesoscale model based studies. Since low resolution regional grids are relatively inexpensive to run, they could be studied to look for specific phenomena or unusual features. In these locations, higher resolution nested grids could be added to properly model the phenomena of interest and/or more closely study the unusual features.

## 6. Profile Construction

For the more sophisticated engineering EDL Monte-Carlo simulations, wind information beyond the simple two parameter analysis was found to be necessary. Instead, the engineering analysis has transitioned to using individual profiles from the mesoscale model results (the engineering work is ongoing and will probably continue up until landing, but is now focused on optimizing the EDL system and lander targeting). The use of specific profiles was primarily to represent the vertical structure in the shear and turbulence, but also to capture the interdependence of the various wind properties. Among other features captured by this method, are the turbulence zones associated with strong shear that are not part of the convective boundary layer.

All of the individual profiles are derived from the MRAMS model [Rafkin and Michaels, this issue] results for consistency in comparing the EDL simulation results between the various sites. The MRAMS model was selected since there were results from all four

potential landing sites and because it explicitly saves the TKE, allowing an estimate of the high frequency turbulence.

Each landing site is represented by a family of 2000 randomly selected profiles. These profiles come from the same ellipse analysis regions and timesteps used in the statistical analysis. A number of profiles from outside the ellipse that show the extreme model tendencies were also processed to study the modeled EDL behavior under extreme conditions.

Each profile consists of the wind velocity versus height in each of the three directions (U, V, and W—eastward, northward, and upwards). Note that the actual model profiles cannot be used directly since they lack the high frequency turbulence that strongly affects the landing success.

### 6.1. High Altitude Winds

One additional request for EDL simulations was to have the wind profiles extend up to an altitude of about 50 km. Unfortunately, the MRAMS mesoscale model as run for the landing site cases only extends to  $\sim 30$  km [Rafkin and Michaels, this issue]. This is solved by using the results from the Ames MGCM (Mars General Circulation Model) [Pollack *et al.*, 1990; Joshi *et al.*, 2000]. The Ames MGCM was chosen since it is the same model MRAMS uses for boundary conditions [Rafkin *et al.*, 2001], thus resulting in a good match between the mesoscale model profiles and the MGCM ones (Figure 7). Note that there is no significant vertical wind from the MGCM, it is assumed to be 0 at all altitudes (the small values are not important for EDL purposes). A cubic spline is used to fit the individual grid points of the MGCM. This was found to give a more reasonable profile than a simple interpolation scheme. In particular, it avoided the high frequency “points” from a linear interpolation (which is effectively what is shown in Figure 7).

For each wind profile, the mesoscale and MGCM profiles are interpolated to the same high resolution final grid. Then a weighted mean profile is selected between 15 km and 30 km. The weight-

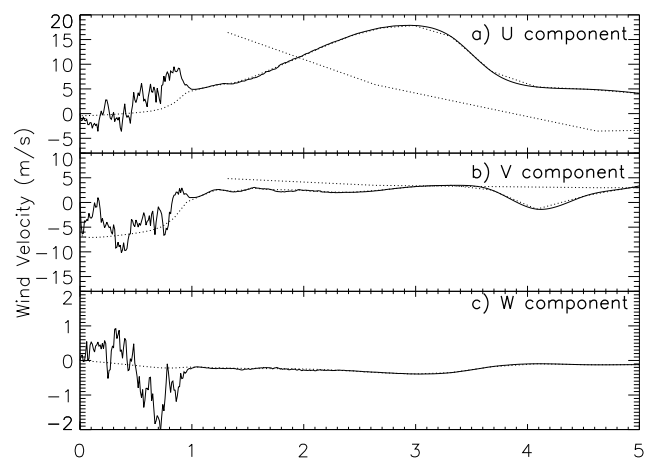


**Figure 8.** Detail of the Profile Generation Process. This figure shows the three wind components ((a)  $u$ , (b)  $v$ , and (c)  $w$ ) as an engineering wind profile is generated. This is the same profile as in Figure 7, but a detail view of the lowest 5 km. Note that the wind velocity changes scale between the two horizontal and the vertical component (and the two horizontal components have a different scale from Figure 7). The solid line is the final generated profile. The dotted line is the MRAMS profile used to generate this profile.

ing varies linearly with altitude to transition between the two model profiles smoothly.

## 6.2. Turbulence Addition

After merging the mesoscale profile with the MGCM profile, it is necessary to account for the high frequency turbulence not represented in the mesoscale model (nor in the MGCM). A power spectral density (PSD—see section 3.1) approach was selected based on the TKE field in the model. While other more sophisticated approaches are possible [Pielke and Pearce, 1994, e.g.], this approach was chosen as adequate and consistent with the earlier analyses.

The high frequency component ( $-5/3$  slope) of the MPF PSD model is used to generate a wind field with high vertical frequency shear over the entire altitude range. This is done independently for each wind direction. It is then scaled by the TKE field for the starting profile from the mesoscale model (Figure 8). This is done using the scaling factor discussed previously. The addition of the high frequency components appears in the deviations from the dotted MRAMS profile below  $\sim 3$  km. The net result is a high frequency component that appears where the mesoscale model shows significant turbulence. This is generally confined to the convective boundary layer but also appears, as expected, in strong, large scale shear zones. This is most noticeable in a few cases at the Gusev Crater site.

## 7. Summary

Overall, estimation of wind speeds and shears has proven to be an important part of ensuring that the MER mission is successful in landing on Mars. To verify the safety of the various sites (as well as comparing them), it was necessary to analyze martian mesoscale wind models for EDL engineering purposes. Given the large data sets produced by the mesoscale models, a number of statistical techniques were applied to reduce the model results to a manageable number of parameters defining their behavior in relation to the key engineering issues.

After examining the results from two models and assessing the current state of mesoscale modeling for Mars, including the lack of observations for validation, we feel that there is an uncertainty on the order of a factor of two in the regions of interest for MER EDL. Since part of the problem is the inability to detect and correct systematic errors in the models, we feel that the comparisons between sites is more discriminatory than the absolute uncertainty, although this will depend somewhat on the degree of similarity between the sites being compared.

The analysis of the winds indicates that from the point of view of winds, the Meridiani Planum site is probably benign (although the strong vertical winds associated with the convective systems may be an issue). The Elysium site is quite similar, with a shallower convective region leading to somewhat higher turbulence. Both Gusev Crater and Isidis Basin sites show stronger effective winds and elevated turbulence. Depending on the exact performance of the EDL system, these are likely to be reasonably safe for landing (although the exact determination will be based on the detailed EDL engineering analyses with the families of profiles). The landing site in Melas Chasma shows strong winds and significant shear and turbulence. It also shows a significant range of wind speeds, causing the tail of the distribution to exceed the landing system's capabilities. Combined,

this results in Melas Chasma probably being a dangerous landing site. It should be noted that unlike many other sites, the Melas Chasma location is likely to be dangerous at most times of the day.

In addition to the engineering evaluation of the landing sites, the statistical techniques have the promise of revealing scientifically interesting aspects of the mesoscale models. One example that developed from the MER analyses is the fact that the convective boundary layer depth is strongly influence by the existence of a prevailing regional wind field. When such exists, the boundary layer tends to be significantly shallower and, as a result of energy conservation, significantly more turbulent.

**Acknowledgments.** We wish to thank Bob Haberle and Jim Schaeffer for the Ames MGCM data. We also wish to thank Rich Zurek, Jeff Barnes, David Crisp, Jim Murphy, Roger Pielke, Nilton Renno and Mike Smith for discussion and suggestions on the work.

This research was carried out at the Jet Propulsion Laboratory, California Institute of Technology, under a contract with the National Aeronautics and Space Administration.

## References

- Crisp, J. M. Adler, J. Matijevic, S. Squyres, R. Arvidson, D. Kass, The Mars Exploration Rover Mission, *J. Geophys. Res.*, this issue, 2003.
- Golombek M., *et al.*, Selection of the Mars Exploration Rover landing sites, *J. Geophys. Res.*, this issue, 2003.
- Holton, James R., *An Introduction to Dynamic Meteorology*, 3<sup>rd</sup> ed., Academic Press, San Diego, 1992.
- Kieffer, H. H., B. M. Jakosky, C. W. Snyder, M. S. Matthews (Eds.) 1992, *Mars*, The University of Arizona, Tucson.
- Joshi M., R. Haberle, J. Hollingsworth, D. Hinson, A comparison of MGS Phase 1 aerobraking radio occultation data and the NASA Ames Mars GCM, *J. Geophys. Res.*, 105(E7), 17,601-17,615, 2000.
- Pielke R. A. and R. P. Pearce, *Mesoscale modeling of the atmosphere*, American Meteorological Society, Boston, 1994.
- Pollack J. B., R. M. Haberle, J. Schaeffer, H. Lee, Simulations of the general circulation of the martian atmosphere 1. Polar processes, *J. Geophys. Res.*, 95(B2), 1447-1473, 1990.
- Rafkin S. C. R., R. M. Haberle, T. I. Michaels, The Mars regional atmospheric modeling system: Model description and selected simulations, *Icarus*, 151, 228-256, 2001
- Rafkin S. C. R. and T. I. Michaels, Meteorological predictions for 2003 Mars Exploration Rover high-priority landing sites, *J. Geophys. Res.*, this issue, 2003.
- Smith, K. S., C. Y. Peng, A. Behboud, Multibody Dynamic Simulation of Mars Pathfinder Entry, Descent and Landing, JPL Document D-13298, 1995.
- Smith, D. E., M. T. Zuber, H. V. Frey, J. B. Garvin, J. W. Head, D. O. Muhleman, G. H. Pettengill, R. J. Phillips, S. C. Solomon, H. J. Zwally, W. B. Banerdt, T. C. Duxbury, M. P. Golombek, F. G. Lemoine, G. A. Neumann, D. D. Rowlands, O. Aharonson, P. G. Ford, A. B. Ivanov, C. L. Johnson, P. J. McGovern, J. B. Abshire, R. S. Afzal, X. L. Sun, Mars Orbiter Laser Altimeter: Experiment summary after the first year of global mapping of Mars, *J. Geophys. Res.*, 106(E10), 23689-23722, 2001.
- Toigo A. D., M. I. Richardson, A mesoscale model for the Martian atmosphere, *J. Geophys. Res.*, 107(E7), 5049, doi:10.1029/2000LE001489, 2002.
- Toigo A. D., M. I. Richardson, The meteorology of proposed Mars Exploration Rover landing sites, *J. Geophys. Res.*, this issue, 2003.

D. M. Kass, 169-237 Jet Propulsion Laboratory, California Institute of Technology, 4800 Oak Grove Drive, Pasadena, CA 91109 (David.M.Kass@jpl.nasa.gov)

(Received \_\_\_\_\_.)